Available online at www.sciencedirect.com

ScienceDirect

Energy Procedia 49 (2014) 2027 – 2036

Energy Procedia

SolarPACES 2013

# Initial experimental and theoretical investigation of solar molten media methane cracking for hydrogen production

D. Paxman[a], S. Trottier[b*], M. Nikoo[b], M. Secanell[a], G. Ordorica-Garcia[c]

[a] *University of Alberta, 4-9 Mechanical Engineering Building, Edmonton, Canada, T6G2G8*
[b] *Alberta Innovates- Technology Futures, 250 Karl Clark Rd., Edmonton, Canada, T6N 1E4*
[c] *National Research Council Canada, 1200 Montreal Road, Ottawa, Canada*, K1A 0R6

**Abstract**

Previous work assessed the fundamental technical and market risks associated with the development and deployment of solar fuels technology in Alberta. It identified methane cracking in solar-molten media as the hydrogen production technology featuring the best combination of technical risk, market acceptance, and breakthrough potential of all the techniques covered in the study. Alberta Innovates – Technology Futures (AITF) plans to advance the technology from a conceptual stage to a proof-of concept over a span of 4 years. The ultimate goal is to design, build and test a prototype solar receiver/reactor in a suitable solar simulator.

The paper outlines the activities to date concerning the initial bench-scale testing of methane cracking in molten media at temperatures ranging from 1023 to 1373 K. The design and construction of an experimental apparatus used to establish the fundamental thermo-chemical performance of the process is presented, along with preliminary results and lessons from the first testing campaign. A transient, non-isothermal, preliminary mathematical model of a reacting bubble within the molten metal has been developed using MATLAB. The model accounts for the chemical reactions, diffusion of the gases in the bubble and heat transfer from the molten metal to the reacting gases. The model can be used to predict the minimum bubble residence time needed to achieve a given hydrogen yield. The simulation tool will be used to numerically estimate methane conversions in the reactor at various conditions.


Selection and peer review by the scientific conference committee of SolarPACES 2013 under responsibility of PSE AG.
Final manuscript published as received without editorial corrections.

*Keywords:* methane cracking; hydrogen production; direct contact pyrolysis; methane decomposition; molten media; liquid metals

* Corresponding author. Tel.: +1-780-450-5469 ; fax: +1-780-450-5083 .
*E-mail address:* stephanie.trottier@albertainnovates.ca


Selection and peer review by the scientific conference committee of SolarPACES 2013 under responsibility of PSE AG.
Final manuscript published as received without editorial corrections.
doi:10.1016/j.egypro.2014.03.215

## 1. Introduction

Canada is the largest per capita hydrogen consumer in the world. The $H_2$ market is dominated by two industries: heavy oil refining/oil sands bitumen upgrading and nitrogen fertilizer production [1] [2]. In the province of Alberta alone in 2010, these industries consumed an estimated 10,000 tonnes $H_2$/day (3.5 million tonnes/y). Hydrogen demand is projected to rise due to the steady expansion of bitumen upgrading operations and increased global fertilizer demand. Nearly all the hydrogen is produced via steam methane reforming (SMR). Although SMR is a commercially mature technology and currently the most economical option, it generates significant $CO_2$ emissions (~8 tonne $CO_2$/tonne $H_2$). Growing domestic and international concerns over the greenhouse gas intensity of Canada's oil/oil sands industry have prompted a search for cleaner $H_2$ production alternatives. Leading options include: electrolysis of water using renewable energy, biomass gasification, SMR with carbon capture and storage (CCS), and solar hydrogen production. Alberta Innovates – Technology Futures (AITF) has identified solar hydrogen production as a significant opportunity for Alberta. Accordingly, a solar hydrogen project was initiated in 2009 aiming to provide a sequential de-risking approach for the successful development and implementation of solar hydrogen production in Alberta. The initial stage of the project consisted of an in-depth technical and market risk analysis [3]. From this analysis, it was decided to focus the de-risking activities on a process utilizing molten metal to crack natural gas at temperatures ranging from 1023-1373K. Serban et al. performed a series of investigations on methane cracking in molten Sn and Pb baths [4]. Fig. 1 is a schematic representation of the concept. After a review of potential metals, Sn was chosen as the bath material for this study because it has a low melting point, is less toxic, has a low vapour pressure, and it allows for a more direct comparison of results with Serban et al. [4]. Other bath materials will be considered in future activities.

In this process, methane or natural gas is injected into a bed of molten metal which is heated by solar energy. The methane will undergo pyrolysis and decarbonize, resulting in solid carbon and hydrogen. The actual reaction sequence is complex but the overall reaction can be simplified as shown in Equation (1) [5].

$$CH_{4(g)} \rightarrow C_{(s)} + 2H_{2(g)} \quad \Delta H = 75\ kJ/mol \tag{1}$$

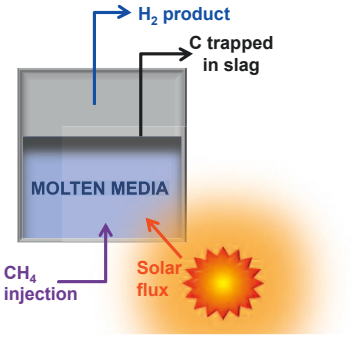


Fig. 1. Schematic of solar molten media methane cracking technology

Thus molten metal methane cracking coupled with solar energy has the benefit of significantly reduced $CO_2$ emissions, in comparison to approximately 8 tonnes of $CO_2$ produced per tonne of $H_2$ in traditional SMR operations. Methane cracking is not dependent on water as a feedstock. The design for heating the reactor could also include burning of natural gas to allow for continuous hydrogen production during the hours of low solar availability.

Another major benefit of this process is the possible simplicity of carbon separation from the product gases due to the density difference of carbon and metal and buoyancy forces [4]. The carbon should rise to the surface of the molten media and form a type of slag. It is envisioned that the carbon slag would be continually removed from a commercial reactor using conventional methods in the metal industry. The carbon formed may be a valuable by-

product. Serban et al. found during experiments that two types of carbons were formed, namely finely divided carbon or soot, and pyrocarbon [6]. The author found that pyrocarbon covered the heated sections of the reactor regardless of the type of molten bath in the reactor when the reactor was vertical with less surface area of tin exposed [6]. Carbon was also deposited at the top surface of the metal [7]. There was no mention of higher order hydrocarbons or toxic polycyclic aromatic hydrocarbons (PAHs) being formed although it is considered possible for these by-products to be formed. This will be investigated in future studies.

The current activities aim to provide an initial proof of concept and gain a better understanding of the impact of various reactor / reaction parameters on the resulting performance of methane cracking. To achieve this, an experimental campaign combined with process mathematical modelling is currently being carried out. This paper highlights current results.

**Nomenclature**

| | |
|---|---|
| $C_{CH4}$ | concentration of methane |
| $c_D$ | drag coefficient |
| $CH_{4conv}$ | methane conversion percentage |
| $CH_{4in}$ | flow rate of methane into reactor |
| $CH_{4out}$ | flow rate of methane out of the reactor |
| $c_p$ | specific heat capacity of the gas bubble |
| $D_g$ | diameter of gas bubble |
| $E_a$ | activation energy |
| $g$ | gravity |
| h | initial depth of bubble in molten Sn |
| $h_f$ | heat of formation of methane |
| $h_{free}$ | free convection coefficient of a gas bubble |
| k | thermal conductivity of the gas bubble |
| $k_o$ | pre-exponential factor in Arrhenius Equation |
| $N_{CH4}$ | flux of methane |
| $P_{atm}$ | atmospheric pressure |
| r | radial distance from center of bubble |
| $r_r$ | rate of reaction |
| $R_0$ | injector tube inner radius or average pore radius of sparger |
| $R$ | ideal gas constant |
| $R_g$ | radius of gas bubble |
| t | time |
| $T_0$ | initial temperature of gas bubble |
| $T_g$ | reactant gas temperature |
| $T_m$ | temperature of bath |
| $T_s$ | Temperature of gas at interface between bubble and bath |
| $\rho_m$ | density of bath |
| $\rho_g$ | density of gas bubble |
| $\sigma$ | surface tension between the gas bubble and molten Sn |
| $v$ | bubble velocity |

### *1.1. Fundamentals of methane cracking*

Various reaction mechanisms have been constructed for methane cracking. The decomposition of methane may be described as a stepwise dehydrogenation at higher temperatures, with ethane as the primary product and ethene, ethyne and benzene as secondary products, as shown in Equation (2) [8].

$$2CH_{4(g)} \rightarrow C_2H_{6(g)} + H_{2(g)} \rightarrow C_2H_{4(g)} + 2H_{2(g)} \rightarrow C_2H_{2(g)} + 3H_{2(g)} \rightarrow 2C_{(s)} + 4H_{2(g)} \quad (2)$$

Detailed models for pyrolysis of methane have identified over 119 reactions [9]. However, to avoid complex analysis of multiple kinetic parameters, the overall decomposition reaction given in Equation (1) is generally accepted. The reaction is generally assumed to be a first order reaction [10], [11] and [12]. Some have reported higher orders [13], [14] and [15]. The first order Arrhenius law is given as

$$r_r = k_0 exp\left(\frac{-E_a}{RT_g}\right) C_{CH_4} \quad (3)$$

Where reported activation energies, $E_a$, range from 65kJ/mol to 433kJ/mol [16].

*1.2. Previous methane cracking processes*

A graphite tubular reactor with indirect solar heating was investigated by Rodat, et al. [5] in 2011. Methane conversion reached 100%, with 88% $H_2$ yield, at 1800K and a residence time above 0.20 s. Co-production of $C_2H_2$ was significant. Wyss, J. et al. [14] developed an indirectly heated fluid-wall aerosol reactor. The reactor is made up of a 5cm outer quartz tube with a concentric 2.4cm diameter inner graphitic tube. An inert gas is injected in the annulus between the tubes to prevent oxidation of the graphite and carbon buildup. Methane was injected into the inner tube. Approximately 70% methane conversion was reached at 2000K. Residence times ranged from 0.06 to 0.12s. Maag, G. et al. [17] presented a directly heated vortex flow reactor. Methane was injected with carbon black particles suspended in the gas. The reactor operated around 1300-1600K, and reached 95% conversion with less than 2.0s residence times. Carbon particles serve as nucleation sites for carbon buildup and absorbed the direct solar energy and improved heating of the feed gas.

In 2003, Serban et al. [4] at the Argonne National Laboratory, USA, presented a novel method of bubbling methane through molten media for hydrogen production. The authors bubbled methane through molten metal in a 35.6cm long by 2.54cm OD 304 SS vertical reactor at temperatures of 873-1073K. Both Sn and Pb were considered for the molten media. Since both metals performed similarly, Pb was abandoned due to toxicity concerns [4]. Different injectors including 0.63cm and 0.32cm SS tubes, and a 0.5 µm sparger from Motts Corporation were investigated. The addition of SiC to the bath to form a solid/liquid mixture was also evaluated by Serban et al. The impact of the different injectors showed that the resulting bubble size of the gas injected in the metal had a very significant effect on the resulting conversion. Methane conversion of 57% was obtained at 1023K with a 0.5 µm sparger and solid/liquid mixture of SiC+Sn [4].

Current studies into molten media cracking are being undertaken by the Karlsruhe Institute of Technology (KIT) and the Institute for Advanced Sustainability Studies (IASS) in Potsdam, Germany [18]. Methane is injected into a bubble column reactor through a porous media. Temperatures up to 1273K are being investigated.

In comparison of current solar cracking technologies, metal has a high thermal conductivity and should remain fairly isothermal throughout the cracking process, leading to significant improvements to the heating of the gaseous methane feed. Methane bubbles will have a high surface contact area, resulting in more efficient heat transfer. Also, because metal has a much higher thermal heat capacitance than a gas, it can dampen solar variations and subject the reactor to less thermal shocking by acting as a thermal storage medium. Furthermore, the carbon is trapped in the molten media, thus effectively reducing carbon plugging in outlet lines.

## 2. Experimental investigation

The initial de-risking campaign was significantly based on the initial investigation carried out by Serban et al. [4]. This was done in order to validate results obtained against previous work. However, the current experimental setup

also allows increased flexibility in the experiments with regards to reactant flow rate, molten media bed and temperature at which the reaction is carried out. The current process is not solarized since it is intended as a highly controllable proof of concept. Solarized reactor design and construction is planned for 2015.

### *2.1. Reactor description*

The reactor, shown in Fig. 2, consists of an alumina crucible, open on one end with a 5.1cm outer diameter and total length of 50.8cm. The reactor is positioned inside a 3 zone furnace. The reaction zone in the reactor is raised to the middle of the furnace where the temperature is most stable, but also to minimize the amount of heated empty reactor space that would exist above a 20.3cm high bath. The top of the reactor is closed with a stainless steel cap and a Viton seal. A k-type thermocouple is inserted in the reactor and sits at a depth of approximately 48.3 cm. The feed gas is comprised of pure methane diluted with nitrogen. The nitrogen is used to allow for mass conservation calculations. Currently, a 6.3cm outer diameter alumina tube is used to inject the gas at the bottom of the reactor in the bed of molten metal. Other injectors, such as porous spargers will also be used as the project progresses. The inlet flow of both nitrogen and methane are controlled using a mass flow controller. All the process parameters are set and measured using a data acquisition system. Sn was selected as the initial molten media and was obtained from Sigma Aldrich. The gas products are analyzed using a Varian CP-4900 micro GC with 10m 55A and PPU columns. The carbon product is analyzed by SEM to characterize its morphology and structure.

Throughout the project, the impact of a number of different parameters on the methane conversion to hydrogen and on the resulting carbon produced will be evaluated. This includes reaction temperature (1023-1373K), injection process either as an open injector or spargers with varying porosity, metal bed presence and height, and residence time of the gas in the reactor.

### *2.2. Experimental results*

The hot commissioning of the reactor has been completed. To this date, a series of experiments from 1023K to 1373K with an empty reactor have been performed to set a baseline for results. The results from cracking with an empty reactor are given in Fig. 3. Conversions as high as 69% were reached at 1373K with feed gas flow rates of both $N_2$ and $CH_4$ set to 15 mL/min. The SEM analysis of carbon formation at both 1373K and 1223K is presented in Fig. 4. XRD analysis showed that the samples were composed of over 99% carbon.

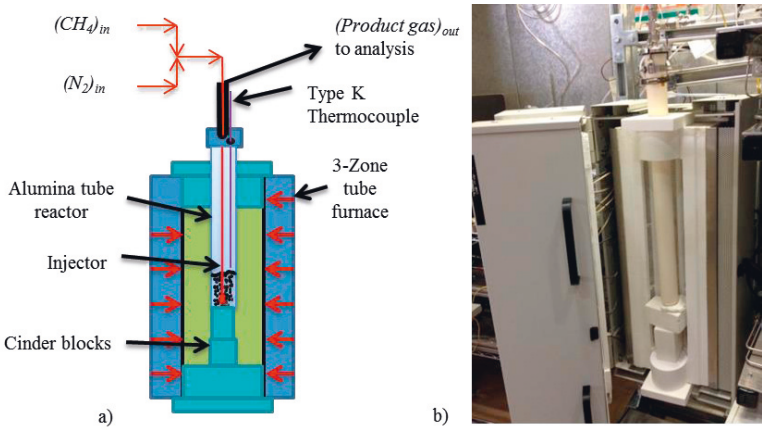


Fig. 2. (a) Schematic of reactor; (b) Picture of reactor.

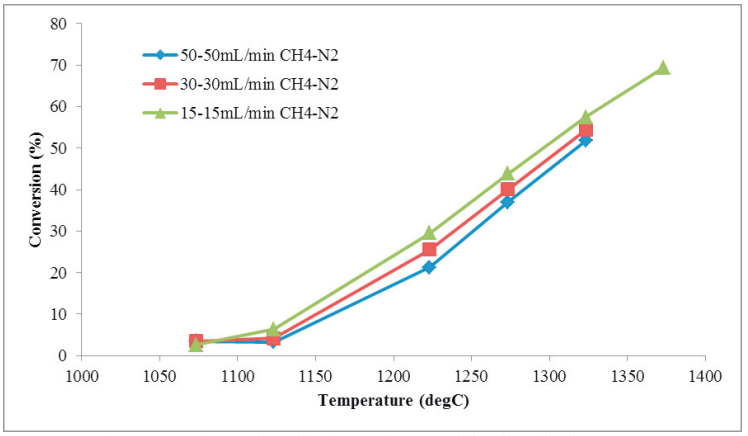


Fig. 3. Experimental results for methane cracking in a blank reactor.

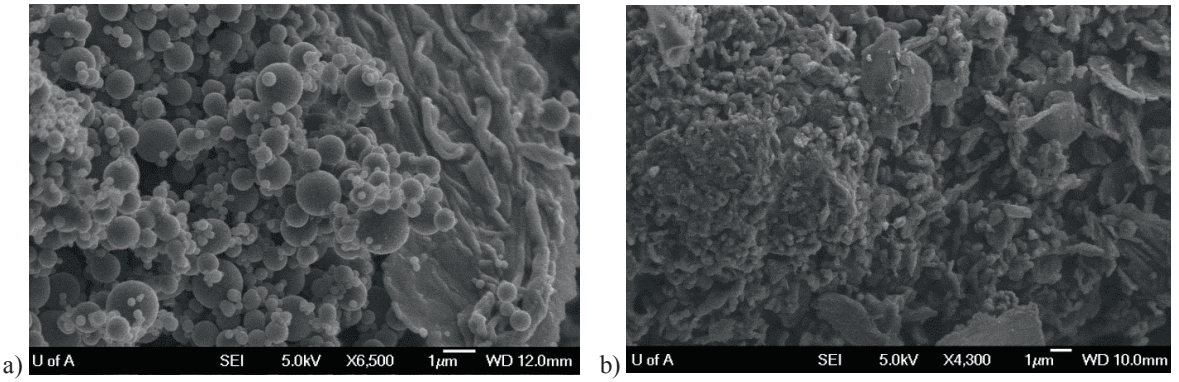


Fig. 4. SEM analysis of carbon formation at (a) 1223K, and (b) 1373K.

The carbons produced at 1223K showed spheres and other striations or formations. The spheres ranged from 100nm to 2μm with the majority being approximately 1μm or less. At 1373K, the carbon atoms appeared to be amalgamated together into flake-like or ribbed formations. The few spheres present seemed to be melded together. The experiments have also produced polycyclic aromatic hydrocarbons, including naphthalene, phenanthrene, fluoranthene and pyrene and their isomers. These compounds have been trapped in the downstream filter.

The next experimental activities will replicate these conditions while bubbling the methane through a molten Sn bed. The impact on the resulting methane conversion will be quantified.

## 3. Modeling

Modeling of the process is also being carried out. As discussed in section 1.3, Serban et al. [4] showed that bubble size has a large effect on the reactor performance. Therefore, two models have been developed using MATLAB. First, a mathematical model to estimate the size and residence time of a bubble in the molten media was developed. Second, a transient, non-isothermal, reactive transport model for $CH_4$ and $H_2$ inside a bubble was created to analyze the concentration of reactants and gaseous products and temperature in the bubble.

### 3.1. Residence time of bubble

The residence time of a bubble in molten media is estimated by calculating the terminal velocity. The model is based on the free body diagram of a bubble shown in Fig. 5. It was assumed that 1) there are no interactions between bubbles; 2) the molten Sn is stationary; 3) the bubble is spherical and smooth and rises vertically; and 4) at low Reynolds numbers ($Re$<1) the drag coefficient can be approximated by $C_D = 16/Re$ [19]. The higher drag coefficient at higher Reynolds numbers is estimated using the dependence of drag coefficients of smooth spheres [20].

The governing equation for bubble rise is then given by Equation (4), and the bubble diameter was estimated using Tate's Law [19], resulting in Equation (5).

$$v = \sqrt{\frac{4gD_g(\rho_m - \rho_g)}{3c_D\rho_g}} \tag{4}$$

$$D_g = \left(\frac{12R_0\sigma}{(\rho_m - \rho_g)g}\right)^{\frac{1}{3}} \tag{5}$$

Tate's law assumes there are no viscous effects, the injector tip is directed upwards in the liquid, the bubbles being formed are spherical, the orifice diameter is small, and that there is no bubble coalescence. Some of these assumptions match with the general assumptions made earlier. However, assumptions such as no viscous effects, and that the injector tip is directed upwards are clearly not met by the experimental setup as described in section 2.1. To this point no other relation to estimate steady state bubble size has been found in literature. Therefore, as a first approximation, it was deemed that this equation would suffice for bubble size albeit there is potential for large error. Other models for dynamic bubble formation can be found in the review by Kulkarni et al. [19].

The surface tension of molten Sn was found in literature to range from 475 J/m$^2$ to 510 J/m$^2$ [21]. Static pressure effects on bubble radius was also investigated and found to be negligible. Based on this model, the rise times in a 20.3cm molten Sn bath for various injectors are shown in Fig. 6. The residence time using a 0.5 μm porous sparger is 7 times longer than using a 6mm sparger, thus showing significant difference between the two injectors used by Serban et al. [4]. The bubble radii for these two cases are 0.028mm and 0.64mm, respectively.

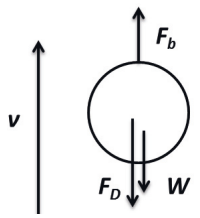


Fig. 5: Free body diagram of a single bubble in molten Sn.

### 3.2. Bubble reaction and heat transfer

A single bubble in molten media was modeled. It was assumed that 1) the bubble is spherical and constant in volume, and does not dissolve into the molten media; 2) the molten Sn is isothermal and remains at operating temperature; 3) the reaction is approximated using the first order Arrhenius equation; 4) the pre-exponential factor and activation energy factors are taken from literature [16] as $k_0$ = 6E11 s$^{-1}$ and $E_a$ =250 kJ mol$^{-1}$. The governing equation for methane dissociation is given in spherical coordinates in Equation (6). The boundary conditions and initial condition are given in Equations (7), (8) and (9), respectively.

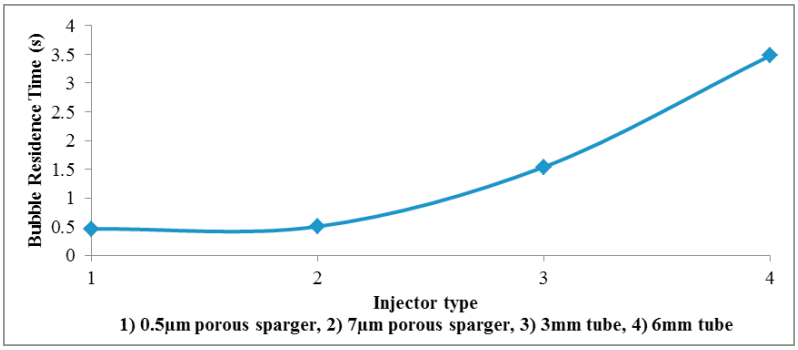


Fig. 6. Bubble residence times for different injectors in a 20.3cm bed height

$$\frac{\partial C_{CH_4}}{\partial \mathrm{t}} = \frac{1}{r^2}\frac{\partial}{\partial r}\left(r^2 D_g \frac{\partial C_{CH_4}}{\partial r}\right) - k_o C_{CH_4} exp\left(\frac{E_a}{RT}\right) \quad (6)$$

$$\mathrm{N}_{CH4} = 0 \qquad \text{at } r = 0 \quad (7)$$

$$\mathrm{N}_{CH4} = 0 \qquad \text{at } r = R_g \quad (8)$$

$$\mathrm{C}_{CH4,0} = \frac{P_{atm} + \rho_m g h}{RT_m} \quad \text{at} \quad t = 0\,\mathrm{s} \quad (9)$$

The governing equation for heat transfer is given in Equation (10), along with the corresponding boundary conditions and initial condition in Equations (11), (12) and (13), respectively.

$$\rho_g c_p \frac{\partial \mathrm{T}_g}{\partial \mathrm{t}} = \frac{1}{r^2}\frac{\partial}{\partial r}\left(r^2 k \frac{\partial T_g}{\partial r}\right) - h_f k_o exp\left(\frac{E_a}{RT}\right) C_{CH_4} \quad (10)$$

$$\frac{\partial \mathrm{T}_g}{\partial \mathrm{r}} = 0 \qquad \text{at } r = 0 \quad (11)$$

$$\frac{\partial \mathrm{T}_g}{\partial \mathrm{r}} = h_{free}(T_b - T_s) \quad \text{at } r = R_g \quad (12)$$

$$\mathrm{T}_0 = 400\mathrm{K} \qquad \text{at } t = 0\,\mathrm{s} \quad (13)$$

The bubble model showed that there were no radial effects for either concentration or heat transfer. Due to the high temperatures and small bubble diameters, the bubble reaches bath temperature nearly instantaneously. Thus the cracking reaction occurs uniformly throughout the bubble. Fig. 7 shows methane conversion over time using the estimated residence times in Section 3.1.

In Fig.7a, it is predicted that methane would be near fully converted after 1 second, whereas in Fig. 7b, methane conversion will only have reached about 40% conversion. The predicted bubble size for a 6mm tube injector is larger than the 0.5 µm porous sparger, which yields lower residence time. In summary, final methane conversions for various injectors in a 20.3cm bed height are given in Fig. 8. Each value was computed using the bubble residence time as predicted using the bubble velocity and diameter model (see Fig. 5).

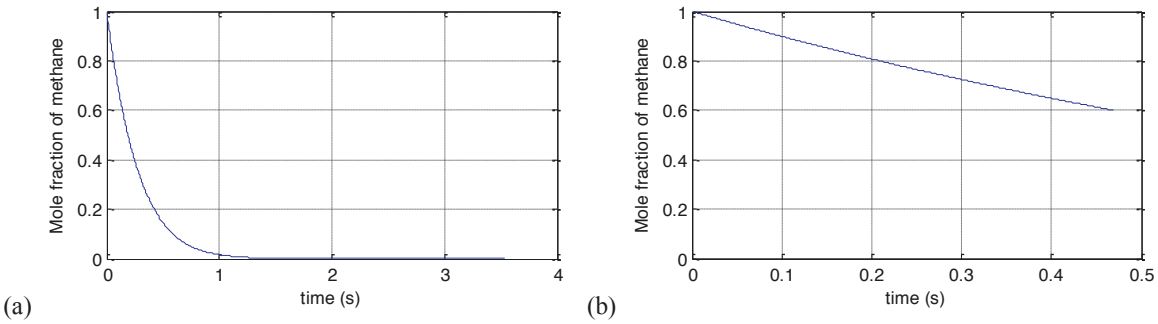


Fig. 7. Conversion of methane at 1173K injecting into a molten Sn bed of 20cm height for a) 0.5µm porous sparger b) 6mm tube injector

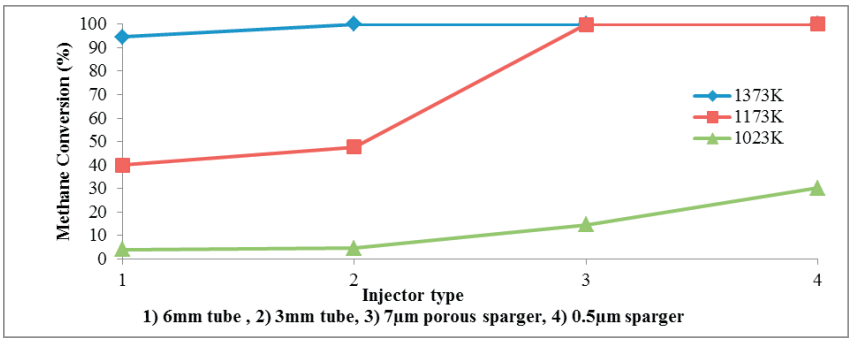


Fig. 8. Methane conversion for various injectors after their respective residence times in a 20.3cm bed

The trend of these curves is as expected i.e. the injectors that create smaller bubbles result in higher conversions and that higher temperatures yield higher conversions. The model predicts 30% conversion for a 0.5 µm sparger in a bath with a 20cm height at 1023K compared to a conversion of 51% obtained experimentally by Serban et al. [4] under the same conditions. Also, for the 6mm tube, the model predicted 4% methane conversion, compared to 8% conversion reported by Serban et al. Discrepancies in these numbers may result from inaccurate estimation of bubble diameter as a result of the first approximation using Tate's law, errors relating to the estimation of bubble rise time by not accounting for bubble coalescence, using kinetic parameters that were not determined by using our experimental results and non-uniform temperature distribution in the molten bath. The errors associated with these results are not quantifiable at this point until further experiments can be performed, and the kinetic parameters can be determined, and the resulting predictions compared against other experimental results. Thus the models will continue to be refined.

## 4. Conclusions

The current project aims to demonstrate an alternative approach for hydrogen production, which is thought to have significant advantages over traditional and solar hydrogen production processes. The molten metal methane cracking process would allow efficient heat transfer to the gas, trapping of the produced carbon and potential energy storage that would limit the impact of solar variation. As well, the process has the potential to produce a valuable by-product as solid carbon. A reactor to carry out a proof of concept was designed, built and commissioned. Initial conversions of 69% in a blank (void of Sn) reactor have been reached at 1373K with feed gas flow rates of both $N_2$ and $CH_4$ set to 15 mL/min.

In addition, preliminary modeling of the process was carried out. The model calculated gas residence time inside molten Sn based on the assumption that the bubble sizes could be estimated using Tate's law. These were correlated with assumed kinetics and resulting conversion rates were calculated for a 20.3cm bed.

Further experiments are planned with the molten metal addition. These will serve to show achievable conversion rates for varying conditions. The produced carbon will also be analyzed to determine potential value. Based on these results, optimization of the process will be carried out. The experiments will also be used to provide accurate inputs for the models.

## References

[1] Suresh B, Hydrogen, Chemical Economics Handbook, SRI Consulting, August 2004
[2] Canadian Hydrogen, Current Status and Future Prospects, Dalcor Consultants Ltd. and Intuit Strategies, August 2004
[3] Ordorica-Garcia et al. Market and technology risks identification for solar fuels implementation in Western Canada. Paper presented at the 2012 SolarPACES Conference. September 11-14, 2102, Marrakech, Morocco.
[4] Serban M, et al. Hydrogen Production by Direct Contact Pyrolysis of Natural Gas, Energy & Fuels 2003;17: 3-705.
[5] Rodat S, Abanades S, and Flamant G. Co-production of hydrogen and carbon black from solar thermal methane splitting in a tubular reactor prototype. Solar Energy 2011;85:4-645.
[6] Serban M, et al. Hydrogen production by direct contact pyrolysis of natural gas, Abstracts Of Papers Of The American Chemical Society 2002; 224: U578.
[7] Lewis MA, et al. Direct Contact Pyrolysis of Methane using Nuclear Reactor Heat, American Nuclear Society. November 11-15, 2001.
[8] Olsvik O, Rokstad O, and Holmen A. Pyrolysis of methane in the presence of hydrogen. Chemical Engineering & Technology 1995;18:5-349.
[9] Billaud F, Gueret C, and Weill J. Thermal decomposition of pure methane at 1263 K. Experiments and mechanistic modelling, Thermochimica Acta 1992; 211:0040-303.
[10] Trommer D. Kinetic investigation of the thermal decomposition of CH4 by direct irradiation of a vortex-flow laden with carbon particles, International Journal of Hydrogen Energy, 2004; 29:6-627.
[11] Rodat S, et al. A pilot-scale solar reactor for the production of hydrogen and carbon black from methane splitting, International Journal of Hydrogen Energy 2010;35:7748.
[12] Patrianakos G, Kostoglou K, and Konstandopoulos A. One-dimensional model of solar thermal reactors for the co-production of hydrogen and carbon black from methane decomposition, International Journal of Hydrogen Energy 2011;36: 1-189.
[13] Dahl JK, Barocas VH, Clough DE, and Weimer AW. Intrinsic kinetics for rapid decomposition of methane in an aerosol flow reactor, International Journal of Hydrogen Energy 2002;27- 377.
[14] Wyss J, et al. Rapid solar-thermal decarbonization of methane in a fluid-wall aerosol flow reactor – Fundamentals and application, International Journal of Chemical Reactor Engineering 2007;5- A69.
[15] Abanades S, and Flamant G. Experimental study and modeling of a high-temperature solar chemical reactor for hydrogen production from methane cracking, International Journal of Hydrogen Energy 2007; 32: 10-1508.
[16] Homayonifar P, Saboohi Y, and Firoozabadi B. Numerical simulation of nano-carbon deposition in the thermal decomposition of methane. International Journal of Hydrogen Energy 2008; 33: 23-7027.
[17] Maag G, Zanganeh G, and Steinfeld A. Solar thermal cracking of methane in a particle-flow reactor for the co-production of hydrogen and carbon, International Journal of Hydrogen Energy 2009; 34: 18-7676.
[18] Karlsruhe Institute of Technology. Hydrogen from Methane without CO2 Emissions. [Online]. Available: http://www.kit.edu/visit/pi_2013_12783.php. [Accessed: 06-Jun-2013].
[19] Kulkarni AA, and Joshi JB. Bubble Formation and Bubble Rise Velocity in Gas−Liquid Systems: A Review, Industrial & Engineering Chemistry Research 2005;44:16-5873.
[20] Herbert Jr. S. et al. Boundary-Layer Theory. Springer, Berlin, 8th ed. edition.
[21] Rhim WK, et al. Noncontact technique for measuring surface tension and viscosity of molten materials using high temperature electrostatic levitation, Review of Scientific Instruments 1999;70:6-2796.